boundary layers developing ahead of the flame. The flame propagates into this self-induced boundary layer, the boundary-layer material burns, and this burned material turns from the wall and is directed into the center of the channel. The subsequent effects of this jetting are both qualitatively and quantitatively different for the two different boundary conditions.

In the case of adiabatic walls, two mechanisms conspire to accelerate the flame to high velocities in the laboratory frame of reference. The first mechanism is that the channel is effectively narrowed by the growth of the boundary layer. The second mechanism is the way in which the boundary-layer material burns: It is jetted into the main body of the reacted material, where it is forced to turn and act as a piston that accelerates the flame. The growth of the boundary layer is found to be self-similar, which agrees with prediction of Stokes's first problem.

Note that the high speed of the flame is measured relative the the laboratory coordinate system. The laminar flame speed is *not* 160 m/s! Rough estimates of the laminar flame speed show that it has not increased very much (if at all) during the process described. The speed of the flame in the laboratory system is what has increased, as well as the outflow velocity and the effective thrust such a system would impart.

The flow with isothermal walls is more complex. The energy loss at the walls induces backward flow behind the flame. The boundary-layer material still turns and jets into the channel as it burns, but now it can turn in two directions, both upstream and downstream. The result is that the flame accelerates less than it does in the adiabatic-wall case, and at times, it even decelerates. This creates an adverse pressure gradient in the boundary layer. Effects that tend to accelerate the flame, such as the effective channel narrowing due to the creation of the boundary layer, are countered by the reverse flow behind the flame. The net result is that the flame oscillates as it moves down the channel. Because of the heat loss at the walls, a quench distance can be defined. The computed quench distance is consistent with a simplified theoretical analysis.

Acknowledgments

This work was sponsored by NASA and the Office of Naval Research. The computations were performed through grants from the Department of Defense High Performance Computing Modernization Office. The authors acknowledge the help of James Holdeman, Alexei Khokhlov, and Moshe Matalon. This work is part of the Ph.D. dissertation of James D. Ott.

References

[1]Ott, J. D., "The Interaction of a Flame and Its Self-Induced Boundary Layer," Ph.D. Dissertation, Dept. of Aerospace Sciences, Univ. of Maryland, 1999.

[2]Ott, J. D., Oran, E. S., and Anderson, J. D., Jr., "The Interaction of a Flame and Its Self-Induced Boundary Layer," NASA CR-1999-209401, 1999.

[3]Mallard, E., and Le Chatelier, H. L., "Recherches Expérimenteles et Théoriques sur la Combustion des Mélanges Gazeux Explosifs," *Les Annales des Mines*, 8th Ser., Vol. 4, 1883, pp. 274–335.

[4]Schmidt, E. H. W., Steinicke, H., and Neubert, U., "Flame and Schlieren Photographs of Combustion Waves in Tubes," *Proceedings of the Combustion Institute*, Vol. 7, 1970, pp. 658–667.

[5]Guénoche, H., "Flame Propagation in Tubes in Closed Vessels," *Nonsteady Flame Propagation*, edited by G. H. Markstein, Pergamon, New York, 1964, Chap. E, pp. 107–135.

[6]Kerampran, S., Desbordes, D., and Veyssière, B., "Study of the Mechanisms of Flame Acceleration in a Tube of Constant Cross-Section," *Combustion Science and Technology*, Vol. 158, 2000, pp. 71–83.

[7]Kerampran, S., Desbordes, D., Veyssiére, B., and Bauwens, L., "Flame Propagation in a Tube from Closed to Open End," AIAA Paper 2001-1082, Jan. 2001.

[8]Daou, J., and Matalon, M., "Flame Propagation in Poiseuille Flow under Adiabatic Conditions," *Combustion and Flame*, Vol. 124, 2001, pp. 337–349.

[9]Daou, J., and Matalon, M., "Influence of Conductive Heat-Losses on the Propagation of Premixed Flames in Channels," *Combustion and Flame*, Vol. 128, 2002, pp. 321–339.

[10]Brailovsky, I., and Sivashinsky, G. I., "Momentum Loss as a Mechanism for Deflagration-to-Detonation Transition," *Combustion Theory and Modelling*, Vol. 2, 1998, pp. 429–447.

[11]Kagan, L., and Sivashinsky, G. I., "The Transition from Deflagration to Detonation in Thin Channels," *Combustion and Flame* (submitted for publication).

[12]Khokhlov, A. M., Oran, E. S., Chtchelkanova, A. Y., and Wheeler, J. C., "Interaction of a Shock with a Sinusoidally Perturbed Flame," *Combustion and Flame*, Vol. 117, 1999, pp. 99–116.

[13]Khokhlov, A. M., Oran, E. S., and Thomas, G. O., "Numerical Simulation of Deflagration-to-Detonation Transition: The Role of Shock–Flame Interactions in Turbulent Flames," *Combustion and Flame*, Vol. 117, 1999, pp. 323–339.

[14]Khokhlov, A. M., and Oran, E. S., "Numerical Simulation of Detonation Initiation in a Flame Brush: The Role of Hot Spots," *Combustion and Flame*, Vol. 119, 1999, pp. 400–416.

[15]Oran, E. S., and Boris, J. P., *Numerical Simulation of Reactive Flow*, 2nd ed., Cambridge Univ. Press, Cambridge, England, U.K., 2001.

[16]Vuillermoz, P., and Oran, E. S., "Mixing Regimes in a Spatially Confined Two-Dimensional Compressible Mixing Layer," *Proceedings of the Royal Society of London, Series A: Mathematical and Physical Sciences*, Vol. 449, 1995, pp. 351–380.

[17]Weber, Y. S., Oran, E. S., Boris, J. P., and Anderson, J. D., Jr., "The Numerical Simulation of Shock Bifurcation near the End Wall in a Shock Tube," *Physics of Fluids*, Vol. 7, 1995, pp. 2475–2488.

[18]Poinsot, T., and Lele, S., "Boundary Conditions for Direct Simulations of Compressible Viscous Flows," *Journal of Computational Physics*, Vol. 101, 1992, pp. 104–129.

[19]Thompson, K., "Time-Dependent Boundary Conditions for Hyperbolic Systems," *Journal of Computational Physics*, Vol. 68, 1987, pp. 1–24.

[20]White, F. M., *Viscous Fluid Flow*, 2nd ed., McGraw–Hill, New York, 1991.

[21]Kuo, K. K., *Principles of Combustion*, Wiley, New York, 1986.

[22]Turns, S. R., *An Introduction to Combustion, Concepts and Applications*, McGraw–Hill, New York, 1996.

G. M. Faeth
Former Editor-in-Chief

Restatement of the Spalart–Allmaras Eddy-Viscosity Model in Strain-Adaptive Formulation

T. Rung,* U. Bunge,* M. Schatz,* and F. Thiele†
Technical University of Berlin,
D-10623 Berlin, Germany

I. Introduction

THE simulation of industrial aerodynamic flows is mostly based on algebraic, one- or two-equation eddy-viscosity models. For highly computing-time-consumptive applications, such as the examination of unsteady flow phenomena around three-dimensional configurations, the one-equation modeling framework is a viable compromise balancing computational effort and predictive accuracy. The Note outlines an effort to extent the predictive realms of the popular Spalart–Allmaras (SA) one-equation model[1] toward nonequilibrium conditions, by means of sensitizing the production term to nonequilibrium effects. The adopted modifications are validated for a range of engineering turbulence-modeling applications.

II. Eddy-Viscosity Transport Model

The proposed strain-adaptive linear Spalart–Allmaras (SALSA) model complies in most parts with the original SA model. The

Received 24 July 2002; revision received 14 January 2003; accepted for publication 15 January 2003.

*Research Associate, Hermann-Föttinger-Institut für Strömungsmechanik.

†Professor, Hermann-Föttinger-Institut für Strömungsmechanik.

present model is based on the eddy-viscosity principle for weakly compressible media with negligible density fluctuations, namely,

$$\overline{u_i u_j} = \frac{2}{3}k\delta_{ij} - \nu_t \tilde{S}_{ij}, \qquad \nu_t = f_{v1}\tilde{\nu}_t, \qquad k = \frac{S^*\nu_t}{\sqrt{c_\mu}}$$

$$c_\mu = 0.09, \qquad \tilde{S}_{ij} = \frac{1}{2}\left[\left(\frac{\partial U_i}{\partial x_j} + \frac{\partial U_j}{\partial x_i}\right)\right] - \frac{1}{3}\frac{\partial U_k}{\partial x_k}\delta_{ij}$$

$$S^* = \sqrt{2\tilde{S}_{ij}\tilde{S}_{ij}} \tag{1}$$

where U_i, $\overline{u_i u_j}$, and $k = \frac{1}{2}\overline{u_i u_i}$ denote the mean velocity, kinematic Reynolds stresses, and turbulence energy, respectively. The eddy-viscosity principle (1) is supplemented by a transport equation for the undamped turbulent (eddy) viscosity $\tilde{\nu}_t$ defined in Eq. (2):

$$\frac{\mathrm{D}\tilde{\nu}_t}{\mathrm{D}t} - \frac{\partial}{\partial x_k}\left[\left(\nu + \frac{\nu_t}{Pr_{\tilde{\nu}_t}}\right)\frac{\partial \tilde{\nu}_t}{\partial x_k}\right] = \underbrace{P_{\tilde{\nu}_t}}_{\text{Production}} + \underbrace{\frac{\partial \tilde{\nu}_t}{\partial x_k}\frac{\partial \tilde{\nu}_t}{\partial x_k}\frac{C_{b2}}{Pr_{\tilde{\nu}_t}}}_{\text{Diffusion}}$$

$$\underbrace{- f_w\left[\frac{\tilde{C}_{b1}}{\kappa^2} + \frac{1 + C_{b2}}{Pr_{\tilde{\nu}_t}}\right]\frac{\tilde{\nu}_t^2}{l_n^2}}_{\text{Dissipation}} \tag{2}$$

The employed damping functions and coefficients read as follows:

$$f_{v1} = \frac{\left(\nu_t^+\right)^3}{C_{v1}^3 + \left(\nu_t^+\right)^3}, \qquad f_w = g\left(\frac{1 + C_{w3}^6}{g^6 + C_{w3}^6}\right)^{\frac{1}{6}}$$

$$g = r[1 + C_{w2}(r^5 - 1)], \qquad r = 1.6\tanh\left[0.7\left(\frac{\Psi}{\tilde{S}}\right)\right]$$

$$\Psi = \sqrt{\frac{\rho_0}{\rho}}\left(\frac{\tilde{\nu}_t}{\kappa^2 l_n^2}\right), \qquad C_{b2} = 0.622, \qquad C_{v1} = 7.1$$

$$C_{w2} = 0.3, \qquad C_{w3} = 2, \qquad \kappa = 0.41, \qquad Pr_{\tilde{\nu}_t} = \frac{2}{3} \tag{3}$$

Here, l_n is the wall-normal distance determined in a customary manner. The definition of the effective velocity gradient $\tilde{S}$ is given by

$$\tilde{S} = S^*\left[\left(1/\nu_t^+\right) + f_{v1}\right], \qquad \nu_t^+ = \tilde{\nu}_t/\nu \tag{4}$$

The choice of the near-wall parameter r follows a route outlined by Edwards and Chandra[2] and is motivated by the more robust behavior experienced for complex industrial applications. The adopted near-wall model slightly alters the predicted skin friction in equilibrium flows. For a flat-plate boundary layer at $Re_\theta = 10^4$, the predicted shape factor H_{12} increases by 1.8%, and the skin friction decreases by the same amount when compared to the SA model.

The specific closure of the production term $P_{\tilde{\nu}_t}$ is outlined in the next section.

III. Production-Term Modification

Among the various recent publications on one-equation models, Menter's[3] rigorous derivation of a generic one-equation model cast in terms of a transport equation for the eddy viscosity ν_t is, perhaps, the most instructive. Based on the application of local-equilibrium assumptions to a two-equation, for example, k–ε, model, Menter's approach provides a keen insight into the one-equation modeling framework, in particular the related coefficients. The procedure reveals that the four most influential production and destruction terms of the two-equation approach collapse into a single production-type term in the one-equation framework, namely,

$$P_{\tilde{\nu}_t} = \tilde{\nu}_t S^*(C_{\varepsilon 2} - C_{\varepsilon 1})(c_\mu S^* k/\varepsilon) \approx \tilde{\nu}_t \tilde{S} C_{b1} \tag{5}$$

The coefficient C_{b1} is thus crucial to the model's predictive performance. As indicated by Eq. (5), C_{b1} is a function of the strain rate and model coefficients. Substituting the employed coefficients of the background k–ε turbulence model by $C_{\varepsilon 1} = 1.45$ and $C_{\varepsilon 2} = 1.9$ and additionally employing $c_\mu S^* k/\varepsilon = \sqrt{(c_\mu)}$, one obtains $C_{b1} = \sqrt{(c_\mu)}(C_{\varepsilon 2} - C_{\varepsilon 1}) = 0.135$, which is close to the original SA model ($C_{b1} = 0.1355$). Both expressions, $(C_{\varepsilon 2} - C_{\varepsilon 1})$ and the anisotropy parameter c_μ, are a function of strain and rotation rate invariants. In general, they both tend to decrease with an increase of strain, which motivates the following modification of the standard coefficient C_{b1}:

$$C_{b1} = 0.1355\sqrt{\Gamma}, \qquad \Gamma = \min[1.25, \max(\gamma, 0.75)]$$

$$\gamma = \max(\alpha_1, \alpha_2), \qquad \alpha_1 = \left[1.01\left(\tilde{\nu}_t/\kappa^2 l_n^2 S^*\right)\right]^{0.65}$$

$$\alpha_2 = \max\left[0, 1 - \tanh\left(\nu_t^+/68\right)\right]^{0.65} \tag{6}$$

Because of the lack of an individual length scale, the approach relies on some heuristics based on the comparison of a mixing length related eddy viscosity with the value obtained from the solution of the transport equation. The modification $\sqrt{\Gamma}$ primarily causes a reduction of production for excessive strains via α_1. Additionally, undesirable wall damping is suppressed by the inclusion of α_2. The limitation of Γ is necessary because of the proportionality of $\tilde{\nu}_t$ and α_1, that is, a decreasing $\tilde{\nu}_t$ causes a decreasing α_1. Because it is closely related to the destruction parameter Ψ, the modification of $\tilde{C}_{b1}$ represents a cross term between production and destruction.

IV. Selected Validational Test Cases and Discussion

The just-mentioned SALSA modification has been validated against a sequence of fundamental building-block flows, for example, channel flows, plane mixing layers, or backward-facing step flows, which are beyond the scope of this Note. Apart from the just-mentioned skin-friction deviations, no significant differences between the SA model and the present suggestion can be observed in equilibrium boundary layers. The investigation of free-shear flows reveals a reduction of 10% of the spreading rate when compared to the SA model. In severe nonequilibrium flows, however, the adjustments show improved results that will be illustrated by three exemplary test cases. The predictive accuracy of Edwards's variant [SA(E)] was generally very close to the SA model for all of the investigated cases.

The first example focuses on a generic wing-body configuration at $\alpha = 12$ deg, $Re = 2.7 \times 10^6$, $Ma = 0.2$, which emerged from an industrial design process.[4] The block-structured computational grid consists of roughly 2.2 million nodes in 48 blocks with Y^+ in the range of $0.3 < Y^+ < 5$ for the points closest to the walls. Figure 1 illustrates the geometry and the pressure distribution. Because the wing is highly optimized for transonic cruise conditions, the flow separates at the leading edge in large areas on the outer wing because of the high angle of attack chosen here. Both one-equation models cannot capture the structure of the flow at separation; nonetheless, Fig. 1 reveals that the results for the SALSA model come close to explicit algebraic stress models.

The second example refers to the results obtained for the simulation of the two-dimensional flow around an ONERA A airfoil at $Re = 2 \times 10^6$, $M = 0.15$, and an angle of attack $\alpha = 13.3$ deg (Ref. 5). The simulation is performed on a C-type, block-structured grid consisting of 281×78 volumes with fixed transition at 12 and 30% chord length on the upper and lower sides, respectively, of the profile. The test case features a laminar (pretransitional) separation in conjunction with a pressure induced trailing-edge separation downstream of $X/C \sim 0.825$ of the suction side. Results depicted by Fig. 2 reveal that the flow reversal is underestimated with any model. The suggested SALSA model is closest to the experiments, due to a better representation of the near-wall distribution of the shear stress $\overline{u'v'}$. In comparison to the SA approach, the present model returns approximately 10% smaller skin-friction values along the equilibrium part of the suction side of the airfoil. Downstream of $X/C = 0.7$, the predicted displacement thickness of the SALSA

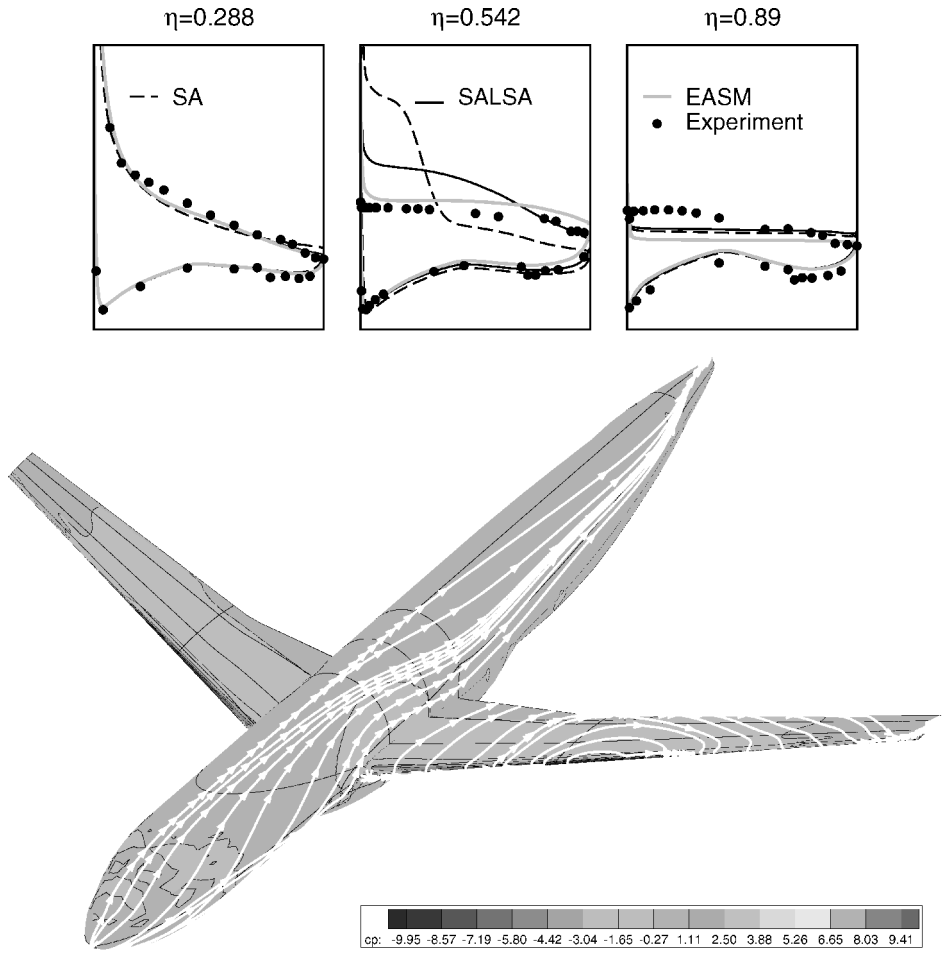

Fig. 1 Flow around generic wing-body configuration: streamlines and pressure coefficient in three selected wing sections $\eta = X/L$.

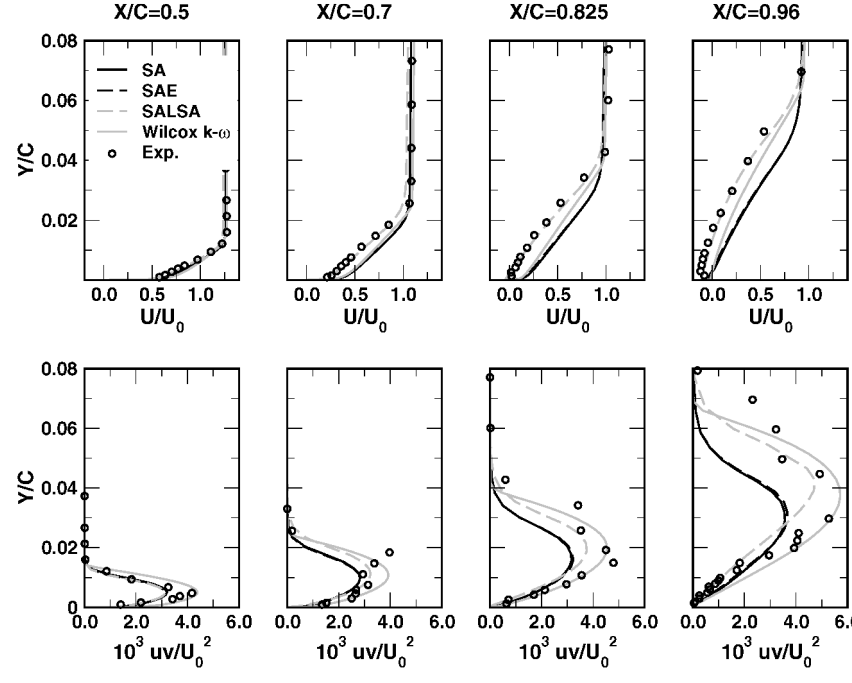

Fig. 2 Flow around ONERA A airfoil ($Re = 2 \times 10^6$, $M = 0.15$, $\alpha = 13.3$ deg): velocity and shear-stress profiles on the suction side.

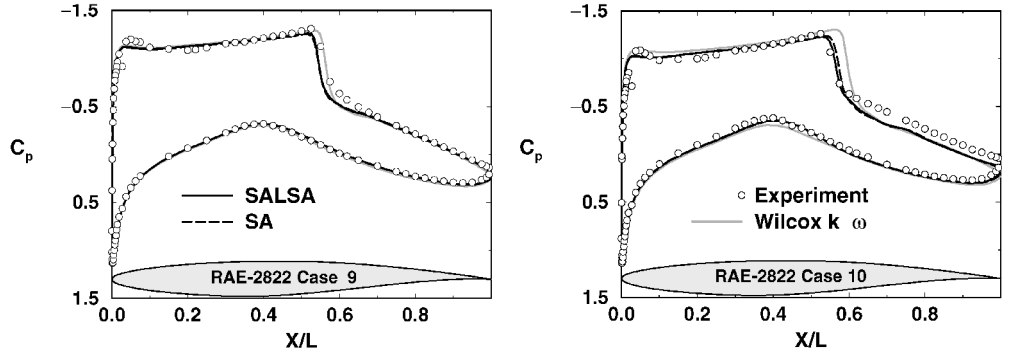

Fig. 3 Transonic flow around RAE-2822 airfoil [case 9 (left), $Re = 6.5 \times 10^6$ and $M = 0.73$; case 10 (left) $Re = 6.2 \times 10^6$, $M = 0.75$, and $\alpha = 2.79$ deg]: distribution of pressure coefficient.

model exceeds the SA value by 90%, which is still more than 10% smaller than experimental data.

Finally, the predicted pressure distributions around a RAE-2822 airfoil[6] exhibiting weak (case 9) and strong (case 10) shock-boundary-layer interaction are presented in Fig. 3. All models reasonably capture the experimental results for less-challenging case 9. For case 10 the considerable predictive differences occur. However, neither model is able to render the correct pressure level on the upper surface in the recovery regime aft of the shock.

V. Conclusions

The present strain-adaptive linear Spalart–Allmaras model provides improved results for nonequilibrium flows while grossly retaining the performance of the Edwards Spalart–Allmaras model in simple boundary-layer and free-shear flows. Although the model cannot be considered universal, it might serve as a good extension of the one-equation modeling framework toward nonequilibrium flows. The suggested sensitization of $\tilde{C}_{b1}$ to variable strain rates is comparatively compact and can easily be implemented in existing codes. Additional corrections, for example, a trip function included or a curvature correction, should remain uninfluenced but have not been validated with the proposed modifications.

Acknowledgments

The authors thank the Commission of the European Communities (UNSI, "Unsteady Viscous Flow in the Context of Fluid-Structure Interaction," Project Ref: BRPR-CT97-0583) and the Deutsche Forschungsgemeinschaft (DFG-SFB 557 "Beeinflussung Komplexer Turbulenter Scherströmunen") for partly funding this research work.

References

[1]Spalart, P. R., and Allmaras, S. R., "A One-Equation Turbulence Model for Aerodynamic Flows," AIAA Paper 92-0439, Jan. 1992.

[2]Edwards, J. R., and Chandra, S., "Comparison of Eddy Viscosity-Transport Turbulence Models for Three-Dimensional, Shock-Separated Flowfields," *AIAA Journal*, Vol. 34, No. 4, 1996, pp. 756–763.

[3]Menter, F., "Eddy Viscosity Transport Equations and Their Relation to the k-ε Model," *Journal of Fluids Engineering*, Vol. 119, 1997, p. 876.

[4]Monsen, E., Franke, M., Rung, T., Aumann, P., and Ronzheimer, A., "Assessment of Advanced Transport-Equation Turbulence Models for Aircraft Aerodynamic Performance Prediction," AIAA Paper 99-3701, June–July 1999.

[5]"EUROVAL–A European Initiative on Validation of CFD Codes," *Notes on Numerical Fluid Mechanics*, Vol. 42, edited by W. Haase, F. Bradsma, E. Elsholz, M. Leschziner, and D. Schwamborn, Vieweg, Braunschweig, Germany, 1993.

[6]Cook, P. H., McDonald, M. A., and Firmin, M. C. P., "Aerofoil 28222-Pressure Distribution, Boundary-Layer and Wake Measurements," AGARD, Rept. AR-138, May 1979.

R. M. C. So
Associate Editor